Journal of Applied Fluid Mechanics, Vol. 15, No. 3, pp. 917-925, 2022.
Available online at www.jafmonline.net, ISSN 1735-3572, EISSN 1735-3645.
https://doi.org/10.47176/jafm.15.03.32911

Numerical Analysis of the Effect of the Non-Sinusoidal Trajectories on the Propulsive Performance of a Bionic Hydrofoil

F. Li, P. Yu†, N. Deng, G. Li and X. Wu

College of Naval Architecture and Ocean Engineering, Dalian Maritime University, Dalian, 116026, China

†*Corresponding Author Email: yupengyao@dlmu.edu.cn*

(Received April 24, 2021; accepted December 19, 2021)

ABSTRACT

Aquatic animals usually generate the effective propulsive force via non-sinusoidally flapping their fins. Inspired by the kinematics of fish, the propulsive characteristics of a NACA012 hydrofoil is numerically studied in this paper. The combination of non-sinusoidal heaving and pitching motions is adopted in the two-dimensional hydrofoil kinematics parameters. The elliptic function and the flattening parameter S are introduced to achieve the varieties of non-sinusoidal periodic motions. The numerical model is established by using the commercial computational fluid dynamic solver STAR-CCM+, and the code is verified by comparing with the published experimental results. The Reynolds number is fixed at 40,000 in all the numerical simulations. The results show that the non-sinusoidal trajectories affect the propulsive performance by affecting the angle of attack (AOA), the hydrodynamics of the foil and the flow structure behind the foil. The non-sinusoidal flapping trajectories can improve significantly the thrust coefficient at the same kinematics parameters compared with the sinusoidal motions in most cases. However, they may reduce the propulsive efficiency. When the values of S are greater than 1, the improvement of thrust coefficient acquired with the non-sinusoidal motions is more obvious. The wake pattern is also discussed which indicates that the strong leading-edge vortices results in the decrease of the propulsive efficiency acquired by the non-sinusoidal trajectories. It is possible to apply the non-sinusoidal motions of a flapping foil to improve propulsive performance of the underwater bionic machine.

Keywords: Flapping hydrofoil; Computational fluid dynamics; Non-sinusoidal motion; Propulsive performance

NOMENCLATURE

$C_{T,time\text{-}averaged}$	time-averaged thrust coefficient	f	oscillation frequency of the foil
$C_{P,time\text{-}averaged}$	time-averaged power input	h_0	heaving amplitude
$\boldsymbol{F}$	volume force	p	pressure
F_x	time-varying force in the thrust direction	α	angle of attack
F_y	time-varying force in the lift direction	η	propulsive efficiency
Re	Reynolds number	θ_0	pitching amplitude
S	flattening parameter	ν	fluid viscosity
St	Strouhal number	ρ	fluid density
T	period of flapping	φ	angle phase between the heaving and pitching motion
U_∞	freestream velocity	ω	angular frequency
c	chord length		

1. INTRODUCTION

After about 10^7 years of the animal evolution in the water environment, aquatic animals have evolved the efficient swimming organs such as whales and dolphins who can control the water flow through the fins to generate fast movement at low energy cost (Fish and Lauder 2006). The imitation of such animals has promoted rapidly the development of

underwater bionic vehicles (Triantafyllou *et al.* 2000). Scholars have conducted many researches on the mechanism of the oscillating foil propulsion and the application in bionic vehicles. The results provided a theoretical basis for the development of underwater bionic vehicles. Gray (1936) first analysed the movement patterns of the aquatic animals such as the dolphins from the theoretical perspective. And the results showed that the dolphins can produce more than 100% propulsive efficiency. Lighthill (1969) showed that the aquatic animals could generate high efficiency in an undulatory manner. At last the author pointed out that the underwater bionic propulsion may be an effective alternative to traditional propeller propulsion.

Many experimental (Triantafyllou *et al.* 1993; Anderson *et al.* 1998; Triantafyllou *et al.* 2004; Lai and Platzer 2015; Nguyen *et al.* 2016) and numerical (Tuncer and Platzer 1996; Ljungqvist 1999; Young and Lai 2004; Young and Lai 2007; Ashraf *et al.* 2011; Benkherouf *et al.* 2011; Olivier and Dumas 2016; Chao *et al.* 2017) studies were conducted to illustrate the fluid mechanism of the thrust generation and proposed some methods to enhance the propulsive thrust force. These works adjusted the kinematic parameters to reveal the optimal propulsive performance, which included the maximum displacement of the foil in the Y direction, the phase angle between the two different motions, the angle of attack (AOA) and the dimensionless Strouhal number (*St*). The optimal propulsive performance and the propulsive efficiency were observed within a narrow range of *St* ($0.2<St<0.45$), which was consistent with the researches on the flying and the aquatics animals (Eloy 2012; Gazzola *et al.* 2014). The optimal phase angle was between 80deg and 100deg. Ashraf *et al.* (2011) and Heathcote *et al.* (2008) studied the geometric parameters of the flapping foil such as the thickness and elasticity of the foil. Ashraf *et al.* (2011) have studied the effect of different Reynolds numbers on a heaving and a combined heaving and pitching motions airfoils. These numerical simulations are carried out under the conditions of fully laminar and fully turbulent flow. The results showed that at *Re*=200, the performance of the thin airfoils is better than the thick airfoils. However, at higher *Re*, the thicker airfoil section had a better improvement in the thrust force and the efficiency. Heathcote *et al.* (2008) analysed the influence of the elasticity of the foil on the bionic propulsion by the experimental methods in a water tunnel. It was found that when $St>0.2$, the optimal flexibility range would result in an increase in the thrust coefficient and the higher efficiency. However, it was found to be disadvantageous to introduce a greater degree of flexibility for the deformable foil bionic propulsion.

The above studies on flapping foil were mostly limited to sinusoidal motion, and the influence of non-sinusoidal motions on the dynamic performance of the flapping foil was very limited (Qi *et al.* 2019; Qadri *et al.* 2019; Xu *et al.* 2021). The works described in Read *et al.* (2003) have concluded that the non-sinusoidal trajectories could achieve better propulsive performance. Kaya and Tuncer (2007) investigated the ways to increase the maximum thrust force and the efficiency of a combined heaving and pitching foil by the non-sinusoidal trajectories. The results shown that the non-sinusoidal motion could enhance significantly the force at expense of efficiency. However, when the flapping path converged to be sinusoidal, the propulsive efficiency was improved. Boudis *et al.* (2019) used the several different non-sinusoidal motions to investigate the way of the thrust generation and the efficiency. The shedding process of the vortices behind the airfoil was used to explain the increase of the thrust force. The results shown that the non-sinusoidal motion always improved the thrust force, however, decrease the maximum propulsive efficiency.

Several useful conclusions were presented to reveal the thrust generation mechanism in previous researches. However, these researches discussed mainly the influence of the motion parameters on the performance of the foil and the discussion about the kinematics of the foil is limited. The medium is air in many studies about the mechanism of the foil such as the work of Boudis *et al.* (2019). Actually, aquatic animals usually produce propulsive force by flapping non-sinusoidally their fins. The researches on the non-sinusoidal hydrofoils with water as the medium are limited. Thus, the present work focuses mainly on the influence of the different non-sinusoidal motions on the bionic propulsion and the hydrodynamics of NACA0012 foil undergoing non-sinusoidal periodic motions. The rest of this paper is organized as follows: First we introduce the computational approach in Section 2. And we present the results and discuss the influence of non-sinusoidal trajectory on propulsive performance in Section 3. Finally, we conclude the paper in Section 4.

2. COMPUTATIONAL APPROACH

2.1 Problem descriptions

Figure 1 shows the combined heaving and pitching trajectories. When the heaving motion and pitching motion are both sinusoidal, the motions of the foil can be expressed as follows:

$$h(t) = h_0 c \cos(\omega t) \tag{1}$$

$$\theta(t) = \theta_0 \cos(\omega t + \varphi) \tag{2}$$

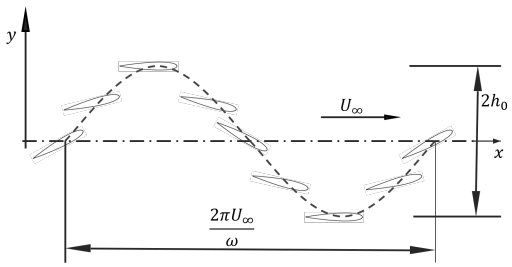

Fig. 1. Spatial sketch of two-dimension flapping foil motion.

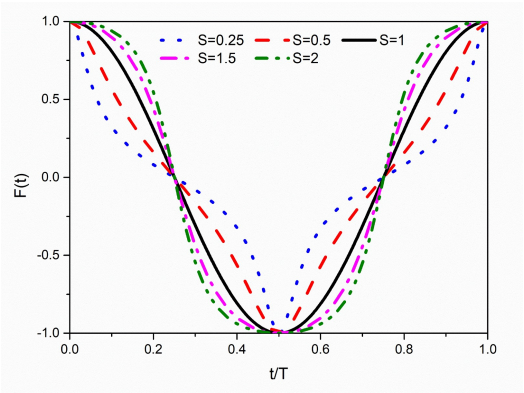

Fig. 2. Flapping trajectories according to different values of the flattening parameter *S*.

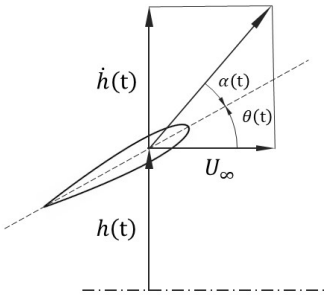

Fig. 3. Sketch of angel of attack *α*(t).

where h_0 is the heaving amplitude, θ_0 is the pitching amplitude, c is the chord length, φ is the angle phase between the heaving and pitching motion, $\omega=2\pi f$ is the angular frequency, f is the oscillation frequency of the flapping foil. The pitch axis is located at 1/3c from the leading edge of the foil. In the present work, we only consider the case φ=90° since the best thrust force and efficiency are acquired between 80deg and 100deg.

Following the works of Boudis *et al.* (2019), the equations for realizing non-sinusoidal trajectories are as follows:

$$h(t)=h_0 c\frac{S\cos(\omega t)}{\sqrt{S^2\cos(\omega t)^2+\sin(\omega t)^2}} \tag{3}$$

$$\theta(t)=\theta_0\frac{S\cos(\omega t+\varphi)}{\sqrt{S^2\cos(\omega t+\varphi)^2+\sin(\omega t+\varphi)^2}} \tag{4}$$

where S is the flattening parameter. Figure 2 shows the non-sinusoidal trajectories, when S=1, the trajectories of the oscillating foil is harmonic. In the present paper, the non-sinusoidal heaving motions and the non-sinusoidal pitching motions are realized by using the same flattening parameter S.

As shown in Fig.3, the effective AOA is defined as the angle between the velocity direction and the chord line as follow equation:

$$\alpha(t)=\tan^{-1}\left(\frac{\dot{h}}{U_\infty}\right)-\theta(t) \tag{5}$$

where U_∞ is the freestream velocity. It is fixed as U_∞=0.2m/s in this paper. In most work, the dimensionless parameter Strouhal number is used to characterize the kinematics of the foil with different parameters. This parameter was defined by Anderson *et al.* (1998) as $St=2cfh_0/U_\infty$. The Reynolds number $Re=\rho cU_\infty/\mu$ is fixed at 40,000 in all the numerical simulations.

The time-averaged thrust coefficient is defined by

$$C_{T,\ mean}=\frac{\frac{1}{T}\int_0^T F_x(t)dt}{0.5\rho cU^2} \tag{6}$$

where F_x is the time-varying force in the thrust direction. T is the period of flapping. The required power during one flapping period is

$$P_{input}=\frac{1}{T}\int_0^T\left[F_y(t)\cdot v(t)+M(t)\cdot\omega(t)\right]dt \tag{7}$$

where F_y is the time-varying force in the lift direction. The time-averaged power input is given by

$$C_{P,\ mean}=\frac{P_{input}}{0.5\rho cU^3} \tag{8}$$

Moreover, the propulsive efficiency can be defined as follows:

$$\eta=\frac{C_{T,mean}}{C_{P,mean}} \tag{9}$$

2.2 Numerical method

In this study, the flow is assumed to be incompressible. The fluid around a two-dimensional (2D) hydrofoil is simulated by solving the Navier–Stokes equations. The governing equations are as follows:

$$\nabla\cdot\boldsymbol{u}=0 \tag{10}$$

$$\frac{\partial\boldsymbol{u}}{\partial t}+(\boldsymbol{u}\cdot\nabla)\boldsymbol{u}=-\frac{1}{\rho}\nabla p+\nu\nabla^2\boldsymbol{u}+\boldsymbol{F} \tag{11}$$

where p is the pressure, $\boldsymbol{F}$ is the volume forces, ρ is the fluid density, u is the fluid velocity, and v is the viscosity.

The hydrofoil is a two-dimensional (2D) symmetric NACA0012 foil profile, and the chord length is 0.1m. The commercial computational fluid dynamic solver STAR-CCM+ is adopted in this paper. The Finite Volume Method is used to discretise the N-S equations. The one equation Spalart-Allmaras model is used in all numerical simulations (Kinsey and Dumas 2012). As shown in Fig. 4, the computational domain is divided into a background zone and an overset zone. According to the works of Chao *et al.* (2019), when the distance of the oscillating foil from the boundary is greater than 20c, the boundary has almost no effect on the hydrofoil. Therefore, the rectangular structured computation domain is created with the dimension of 60c×40c. The overset mesh method is used to

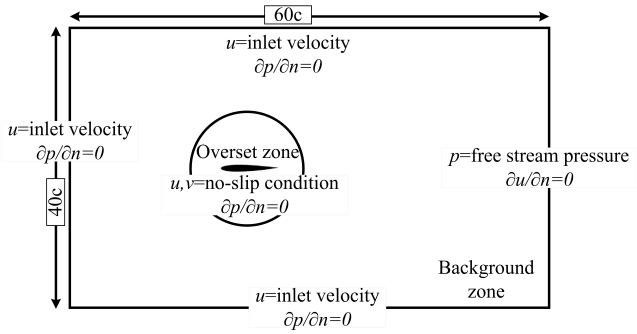

Fig. 4. Computational domain and boundary conditions.

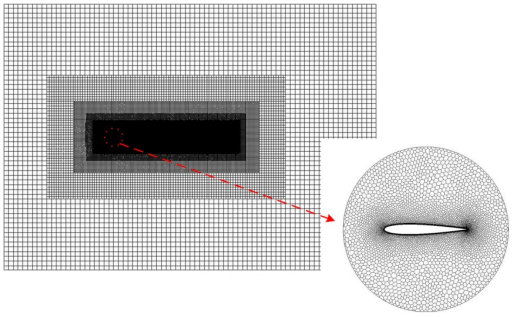

Fig. 5. Mesh condition around the foil.

Table 1 Characteristics of three different computational domains

Grid name	Number of points on foil	Number of cells
Coarse grid	200	3×10^4
Medium grid	400	10×10^4
Fine grid	600	22×10^4

simulate the motions of the foil. The overset zone is a circle with a radius of 1*c*. The boundary conditions at inlet are zero gradient pressure and the Reynolds number determines the fluid velocity. The outlet velocity is zero gradient and the pressure are set to freestream pressure. The no-slip condition is imposed (Boudis *et al.* 2019) on the foil surface. Figure 5 shows that the total number of grids in selected computational domain is approximately 1×10^5 with 400 nodes around the foil. In order to ensure y+⩽1, the height of the first layer grid is $10^{-5}c$.

2.3 Grid and time step sensitivity

To evaluate the sensitivity of the hydrodynamics to the computational domain, we select three mesh size grids with the different number of points on the foil to simulate numerically the hydrodynamic at the same conditions. These series of simulations are carried out with the following parameters: h_0=0.175*c*, *Re*=2×10^4, *St*=0.3, *S*=0.25, *t*=*T*/2500. Table 1 shows the details of the three grids.

Figure 6 displays the history of the thrust coefficient acquired from the three grids over per unit period. The number of grid nodes on the flapping foil surface has little effect on the

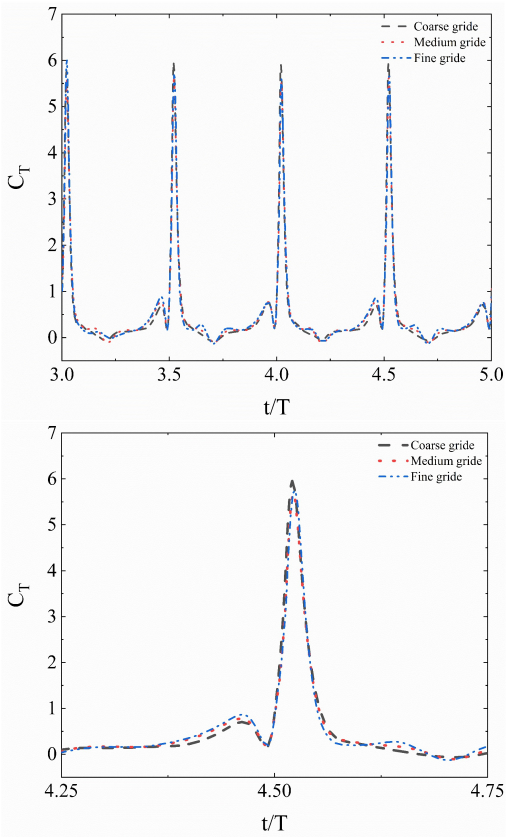

Fig. 6. Grid independence study.

calculated results near the trough of the thrust coefficient. And the difference between the results acquired from the Medium grid and the Fine grid is insignificant at the peak of the thrust coefficient. The existed difference of the thrust coefficient is only 1% that can be assumed the mesh has converged. By contrast, the result of Coarse grid is different at the peak which is 5.33%. Medium grid is selected as the optimum computational mesh for subsequent calculations. Next, we perform the time step sensitivity analysis using the following three different time steps: *T*/1000, *T*/2500, *T*/4000. Figure 7 shows the history of thrust coefficient over per unit period acquired with the three time steps. It can be seen that the results acquired with *T*/2500 are closed to that acquired with *T*/4000. While the results acquired with *T*/1000 are quite different from the other two results. Thus, we select the time-

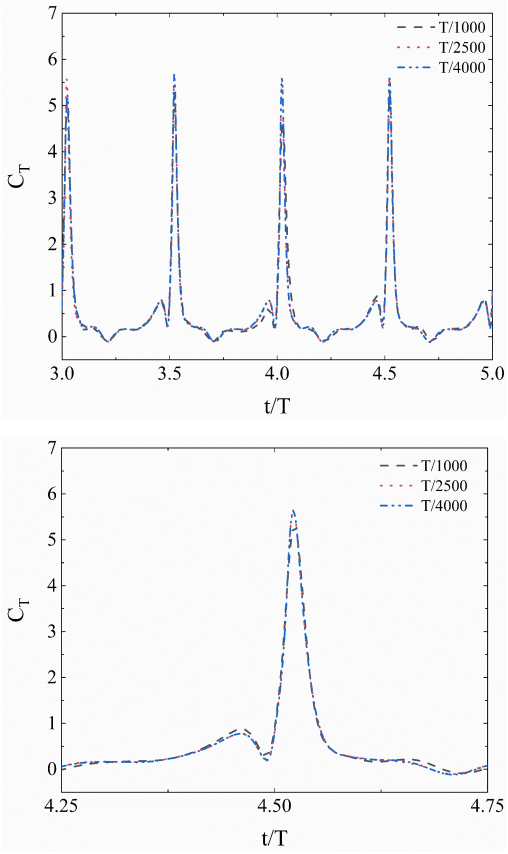

Fig. 7. Time-step independence study.

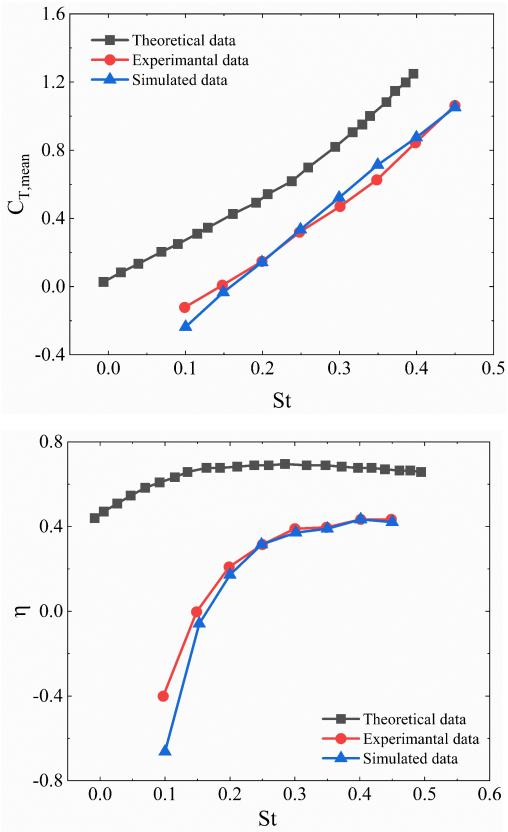

Fig. 8. Comparison of the time-averaged thrust coefficient and propulsive efficiency.

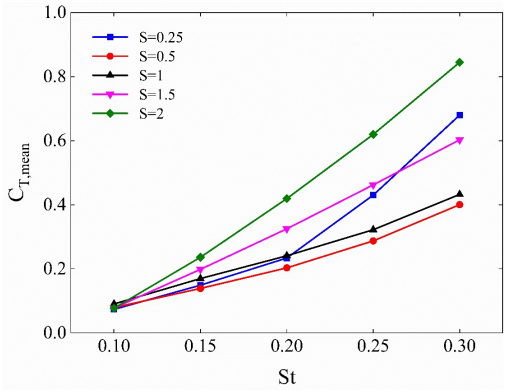

Fig. 9. Thrust coefficient versus Strouhal numbers *St* for different flattening parameter *S*.

step *T*/2500 and the Medium grid as the fixed parameter for following simulations in this paper.

2.4 Code validation

The thrust force and the efficiency are simulated by the following parameters: U_∞=0.4m/s, h_0=0.75*c*, α_{max}=30°. The time-averaged thrust coefficient and the efficiency acquired in this section are compared to the experimental data acquired at the MIT Tow Tank by Schouveiler *et al.* (2005) and the theoretical value by Lighthill (1970). Figure 8 displays the results with *St* in 0.1~0.4. Lighthill (1970) proposed the two-dimensional unsteady aerofoil theory which overestimated the thrust coefficient and the efficiency. However, the numerical results acquired by using the numerical method proposed in this paper are much better agreement with the experimental data acquired by Schouveiler *et al.* (2005). The numerical simulation method established in this study is feasible and effective.

3. RESULTS AND DISCUSSION

In this section, the effect of the non-sinusoidal flapping trajectories on the effective AOA, the hydrodynamics, the flow structure and the propulsive performance is systematically investigated. The kinetics parameters of the hydrofoil are fixed as: h_0=0.75*c*, α_{max}=15°, φ=90°, *Re*=4×104, 0.1≤*St*≤0.3.

3.1 Effect on the propulsive performance

The influence of Strouhal number *St* and the flattening parameter *S* on the overall time-averaged thrust force and the efficiency of the hydrofoil is discussed in this section.

In Fig. 9 and Fig. 10, Strouhal number *St* and the flattening parameter *S* have a significant influence on the time-averaged thrust force. The numerical simulation results increase with the increasing of Strouhal number *St* in Fig. 9. For *S*=0.25, the time-averaged thrust coefficient is enhanced dramatically at high *St*, especially greater than 0.2. As shown in Fig. 10, the effect of the different values of the flattening parameter *S* is slight for *St*=0.1. However, the enhancement becomes more obvious with the

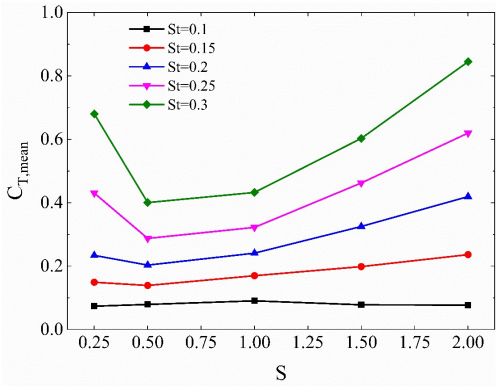

Fig. 10. Thrust coefficient versus flattening parameters *S* for different Strouhal numbers *St*.

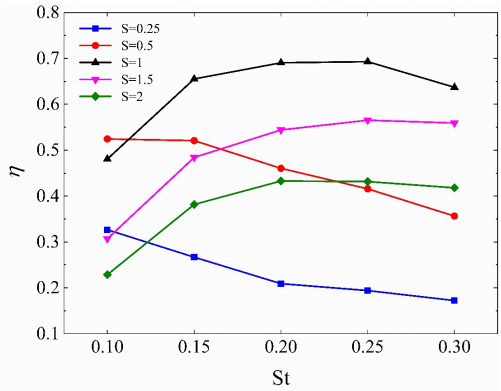

Fig. 11. Propulsive efficiency versus Strouhal numbers *St* for different flattening parameter *S*.

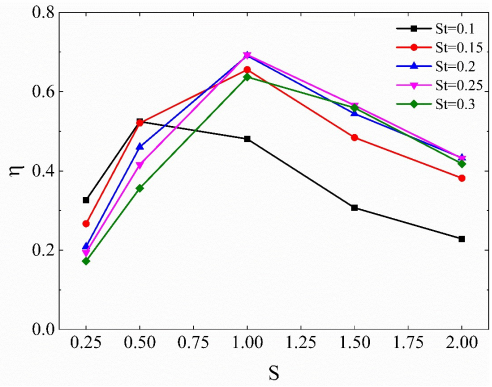

Fig. 12. Propulsive efficiency versus flattening parameters *S* for different Strouhal numbers *St*.

increasing of Strouhal number *St*. The time-averaged thrust coefficient acquired with *S*=0.25, 1.5 and 2 are always better that that acquired with *S*=1 for each Strouhal number. For *S*=0.25 and *S*=2, the effect of non-sinusoidal trajectories on the time-averaged coefficient is greatest. The values of *S*=0.25 and *S*=2 are 0.68 and 0.85, respectively, which are improved by 59% and 98% compared with sinusoidal trajectories.

As shown in Fig. 11. and Fig. 12., the variation trends of the efficiency with Strouhal number *St* and

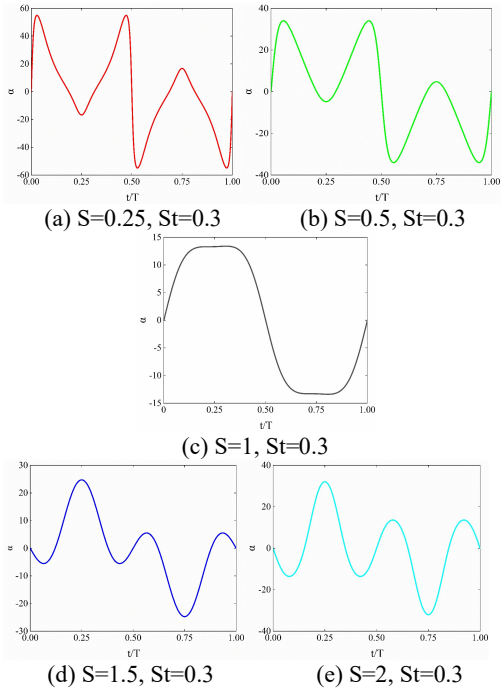

(a) S=0.25, St=0.3 (b) S=0.5, St=0.3

(c) S=1, St=0.3

(d) S=1.5, St=0.3 (e) S=2, St=0.3

Fig. 13. Angle of attack in one flapping period for different flattening parameter *S*.

the flattening parameters *S* are presented. The propulsive efficiency decreases slightly with the increasing of *St* at *S*=0.25 and *S*=0.5 in Fig.11. The maximum efficiency is achieved at *St*=0.1. The efficiency increases steadily until *St*=0.25 and decreases gradually beyond *St*=0.25 for the cases of *S*=1, *S*=1.5 and *S*=2. In Fig. 12, the propulsive efficiency increases until S=1 and decreases beyond *S* =1 for the cases of *St*=0.15, 0.2, 0.25 and 0.3. The maximum propulsive efficiency is always acquired at *S*=1 except at *St*=0.1. The values of the maximum propulsive efficiency are all above 60% while the maximum propulsive efficiency is 52% at *St*=0.1. The non-sinusoidal trajectories of the flapping foil can improve the time-averaged thrust coefficient and they also can decrease the propulsive efficiency compared with the sinusoidal trajectories in most cases.

3.2 Effect on effective angle of attack

The influence of non-sinusoidal trajectories of the hydrofoil on AOA is considered in this section. The Strouhal number is selected to *St*=0.3 (corresponding to maximum thrust coefficient). Figure 13 displays the temporal variation of the effective AOA over per unit cycle for different values of *S*. In Fig.13(c), the effective AOA increases as increasing of heaving velocity, and it reduces as the heaving velocity decreases. Some irregular changes appear at t=0.25T,t=0.75T and the maximum AOA is approximately 14°. In the other words, it is expected that two extrema over one flapping cycle are shown at AOA profile when it is cosine-type. When the hydrofoil is at the middle height position, a maximum and a minimum are

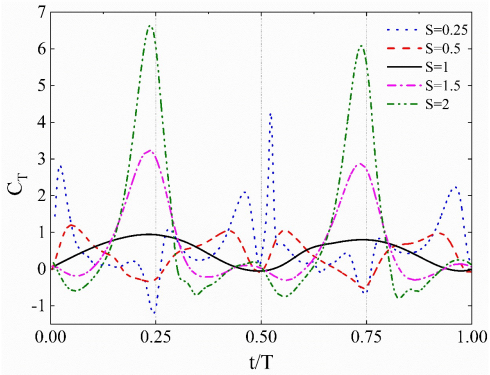

Fig. 14. Time variation of C_T under the effect of non-sinusoidal motions at St=0.3.

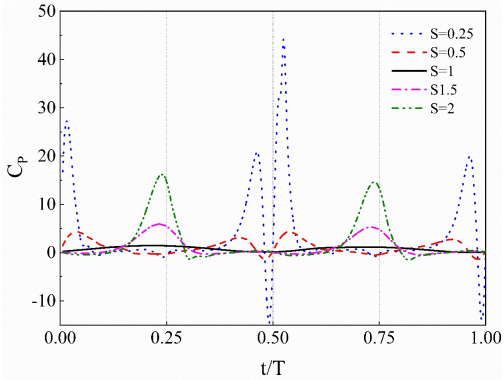

Fig. 15. Time variation of C_P under the effect of non-sinusoidal motions at St=0.3.

displayed alternately. It is consistent with the AOA profiles presented in the work studied by Schouveiler *et al.* (2005). As shown in Fig.13(d), it is similar to the harmonic behaviour at S=1.5 that the maximum AOA is approximately 25° and two new extrema are shown at vicinity of t=0.25T,t=0.75T in the AOA profiles. These irregular changes are more obvious at S=2 and the maximum AOA can reach 30°. From Fig. 13(c)-(e), it can be predicted that the maximum AOA will increase with the increase of the flattening parameter S in the case of S>1. In Fig. 13(b), the maximum AOA is no longer shown at near t=0.25T,t=0.75T at S=0.5 but at vicinity of t=0.5T,t=1T and it is approximate 33°. The maximum AOA appears closer to t=0.5T,t=1T at S=0.25 and it is approximate 55°.

The thrust and the propulsive efficiency can be improved greatly by controlling the AOA profiles (Hover *et al.* 2004). Xiao and Liao (2010) used the computational method to reveal the enhancement of effective AOA on propulsive performance of a combined pitching and heaving NACA0012 foil. The cosine AOA profile could effectively remove the degradation of the thrust force and efficient with sinusoidal heaving or pitching motion. The effect of the effective AOA on the leading-edge vortices and the wake of the hydrofoil is significantly strong. A strong vortices structure behind the foil is generated with the non-sinusoidal trajectories which is discussed in detail in section 3.4.

3.3 Effect on the hydrodynamics

To deeply study the influence of non-sinusoidal trajectories on the thrust generation mechanism of the foil, the time-varying thrust coefficient and the power coefficient over per unit cycle are analysed in this section. The values of St are fixed at St=0.3 in this section. The time-varying thrust coefficient are presented in Fig.14. It is noted that the variation of C_T is non-sinusoidal and two peaks are observed in one typical cycle for the cases of S=1.5 and S=2, which are shown at the vicinity of t=0.25T,t=0.75T.

The oscillating foil moves to the mean position at t=0.25T,t=0.75T and the maximum AOA (Fig.13) results in the maximum thrust force. The time-varying thrust coefficient is quite consistent with the variation of time-varying effective AOA. In other words, the variation trends of time-varying and AOA are similar. When the AOA reaches the maximum, the time-varying thrust coefficient is also the highest. The peaks of the time-varying thrust coefficient acquired by the non-sinusoidal trajectories are much larger than that by the sinusoidal trajectories. The time-varying power coefficient is presented in Fig. 15. The peaks of the time-varying power coefficient at S=0.25 is the highest and the change is most complicated, which is the reason why its propulsive efficiency is the lowest among all non-sinusoidal trajectories.

3.4 Effect on the flow structure

The formation of the leading-edge vortices, the shedding process and the flow structure behind the trailing edge are closely related to the thrust generated by the hydrofoil and the propulsive efficiency (Xiao and Liao 2010). The mechanism of thrust generated by the flapping foil is further analysed by visualising the vortices shedding pattern.

Figure 16 shows the vorticity field of different flattening parameter S for St=0.3 and the vertical displacement of the foil is $h(t)$=0 at t=0.25T. It can be seen that the vortices shedding is more obvious for the non-sinusoidal motions. This is mainly due to the velocity of the foil with non-sinusoidal trajectories is faster than that with sinusoidal trajectories, which can also be found in the AOA profiles of Fig. 13. In Fig.16(b)-(c), the strong leading-edge vortices cause interference to the wake structure behind the flapping foil. The propulsive efficiency is much smaller than the sinusoidal trajectories for S<1. The leading-edge vortices change the efficiency by affecting the pressure distribution on the foil surface and the interference they cause to the trailing edge vortices system behind the foil. (Lewin and Haj-Hariri 2003). It is studied that reducing the intensity of the leading-edge vortices is essential to acquire high efficiency, which is achieved by reducing the AOA (Pedro *et al.* 2003; Tuncer and Kaya 2005). However, such a small effective AOA will result in a small thrust coefficient, and it is necessary to find a balance

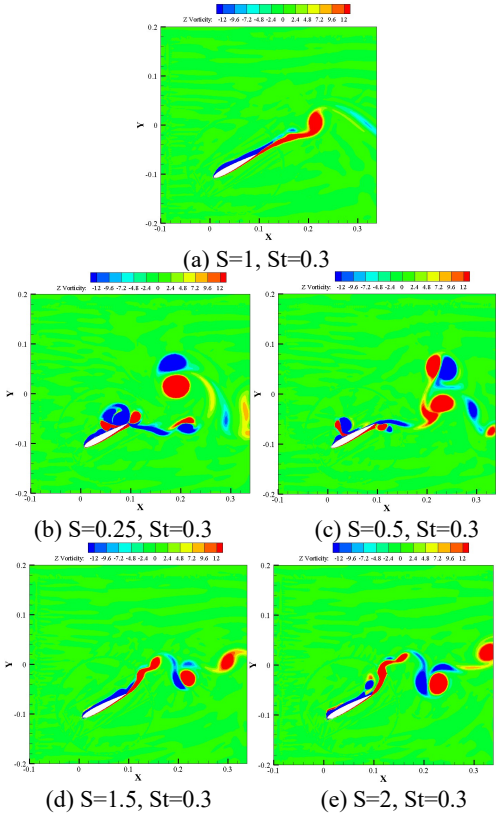

(a) S=1, St=0.3

(b) S=0.25, St=0.3 (c) S=0.5, St=0.3

(d) S=1.5, St=0.3 (e) S=2, St=0.3

Fig. 16. Vorticity field for different flattening parameter *S*.

between high thrust force and high efficiency (Platzer *et al.* 2008).

4. CONCLUSIONS

In the present study, we carry out a systemic numerical study to investigate the fluid dynamics around the oscillating foil to understand the force generation and wake structures of the hydrofoil. The Reynolds number is set to 40,000 and the fluid in the flow regime is supposed to be incompressible. The commercial computational fluid dynamic solver STAR-CCM+ is used to perform the numerical simulations in the present work. The flattening parameter *S* is used to define the non-sinusoidal flapping trajectories of the foil. The results show that the non-sinusoidal trajectories can affect significantly the flow structure and improve the thrust force by enhancing the vortices behind the foil.

The non-sinusoidal motion trajectories cause the maximum AOA increase and the irregular changes become more obvious. The non-sinusoidal motion trajectories have a positive effect on the time-varying thrust coefficient by changing the angle of attack profiles. On the other hand, in lower Strouhal number, the non-sinusoidal trajectories of the foil have only a slight effect on the time-averaged thrust coefficient. Considering high Strouhal number, the time-averaged thrust coefficient increases significantly by using the different flattening parameters *S*. Under the optimal parameter combination, the maximum time-averaged thrust coefficient is 0.85 which is improved by 98% compared with the sinusoidal motion. However, the efficiency acquired with sinusoidal trajectories is always better than that acquired by the non-sinusoidal trajectories except for *St*=0.1. Eventually, we can conclude that the non-sinusoidal trajectories can significantly enhance the thrust coefficient at the expense of the propulsive efficiency. The improvement of the propulsive performance is also discussed in more details by analysing the flow structures downstream the foil.

ACKNOWLEDGEMENTS

This work was supported by National Key Research and Development Program of China (Grant No. 2016YFC0301500); Natural Science Foundation of Liaoning Province in 2020 (Grant No. 2020-MS-125); State Key Laboratory of Ocean Engineering, Shanghai Jiao Tong University (Grant No. 1904).

REFERENCES

Anderson, J. M., K. Streitlien and D. S. Barrett (1998). Oscillating foils of high propulsive efficiency. *Journal of Fluid Mechanics* 360(360), 41-72.

Ashraf, M. A., J. Young and J. C. S. Lai (2011). Reynolds number, thickness and camber effects on flapping airfoil propulsion. *Journal of Fluids and Structures* 27(2), 145-160.

Benkherouf, T., M. Mekadem, H. Oualli, S. Hanchi, L. Keirsbulck and L. Labraga (2011). Efficiency of an auto-propelled flapping airfoil. *Journal of Fluids and Structures* 27(4), 552-566.

Boudis, A., A. C. Bayeul-Laine, A. Benzaoui, H. Oualli, O. Guerri and O. Coutier-Delgosha (2019). Numerical Investigation of the Effects of Nonsinusoidal Motion Trajectories on the Propulsion Mechanisms of a Flapping Airfoil. *Journal of Fluids Engineering* 141(4), Article 041106.

Chao, L.-M., G. Pan, D. Zhang and G.-X. Yan (2019). Numerical investigations on the force generation and wake structures of a nonsinusoidal pitching foil. *Journal of Fluids and Structures* 85, 27-39.

Eloy, C. (2012). Optimal Strouhal number for swimming animals. *Journal of Fluids and Structures* 30(2), 205-218.

Fish, F. E. and G. V. Lauder (2006). Passive and active flow control by swimming fishes and mammals. *Annual Review of Fluid Mechanics* 38(1), 193-224.

Gazzola, M., M. Argentina and L. Mahadevan (2014). Scaling macroscopic aquatic locomotion. *Nature Physics* 10(10), 758-761.

Gray, J. (1936). Studies in Animal Locomotion, VI. The Propulsive Powers of the Dolphin. *Journal*

of Experimental Biology 13(2), 192-199.

Heathcote, S., Z. Wang and I. Gursul (2008). Effect of spanwise flexibility on flapping wing propulsion. *Journal of Fluids and Structures* 24(2), 183-199.

Hover, F. S., O. Haugsdal and M. S. Triantafyllou (2004). Effect of angle of attack profiles in flapping foil propulsion. *Journal of Fluids and Structures* 19(1), 37-47.

Kaya, M. and I. H. Tuncer (2007). Nonsinusoidal path optimization of a flapping airfoil. *AIAA Journal* 45(8), 2075-2082.

Kinsey, T. and G. Dumas (2012). Computational Fluid Dynamics Analysis of a Hydrokinetic Turbine Based on Oscillating Hydrofoils. *Journal of Fluids Engineering* 134(2), Article 021104.

Lai, J. C. S. and M. F. Platzer (2015). Jet Characteristics of a Plunging Airfoil. *AIAA Journal* 37(12), 1529-1537.

Lewin, G. C. and H. Haj-Hariri (2003). Modelling thrust generation of a two-dimensional heaving airfoil in a viscous flow. *Journal of Fluid Mechanics* 492, 339-362.

Lighthill, M. J. (1969). Hydromechanics of Aquatic Animal Propulsion. *Annual Review of Fluid Mechanics* 1(1), 413-446.

Lighthill, M. J. (1970). Aquatic animal propulsion of high hydromechanical efficiency. *Journal of Fluid Mechanics* 44(2), 265-301.

Ljungqvist, B. D. (1999). Flapping and flexible wings for biological and micro air vehicles. *Progress in Aerospace Sciences* 35(5), 455-505.

Nguyen, T. A., H. Vu Phan, T. K. L. Au, H. C. J. B. Park (2016). Experimental study on thrust and power of flapping-wing system based on rack-pinion mechanism. *Bioinspiration and Biomimetics* 11(4), 046001.

Olivier, M. and G. Dumas (2016). Effects of mass and chordwise flexibility on 2D self-propelled flapping wings. *Journal of Fluids and Structures* 64, 46-66.

Pedro, G., A. Suleman and N. Djilali (2003). A numerical study of the propulsive efficiency of a flapping hydrofoil. *International Journal for Numerical Methods in Fluids* 42(5), 493-526.

Platzer, M. F., K. D. Jones, J. Young and J. C. S. Lai (2008). Flapping-wing aerodynamics: Progress and challenges. *AIAA Journal* 46(9), 2136-2149.

Qadri, M. N. M., A. Shahzad, F. Zhao and H. Tang (2019). An Experimental Investigation of a Passively Flapping Foil in Energy Harvesting Mode. *Journal of Applied Fluid Mechanics* 12(5), 1547-1561.

Qi, Z., J. Zhai, G. Lie and J. Peng (2019). Effects of non-sinusoidal pitching motion on the propulsion performance of an oscillating foil. *PloS One* 14(7), Article e0218832.

Read, D. A., F. S. Hover and M. S. Triantafyllou (2003). Forces on oscillating foils for propulsion and maneuvering. *Journal of Fluids and Structures* 17(1), 163-183.

Schouveiler, L., F. S. Hover and M. S. Triantafyllou (2005). Performance of flapping foil propulsion. *Journal of Fluids and Structures* 20(7), 949-959.

Triantafyllou, G. S., M. S. Triantafyllou and M. A. Grosenbaugh (1993). Optimal Thrust Development in Oscillating Foils with Application to Fish Propulsion. *Journal of Fluids and Structures* 7(2), 205-224.

Triantafyllou, M. S., G. S. Triantafyllou and D. K. P. Yue (2000). Hydrodynamics of fishlike swimming. *Annual Review of Fluid Mechanics* 32, 33.

Triantafyllou, M. S., A. H. Techet and F. S. Hover (2004). Review of experimental work in biomimetic foils. *IEEE Journal of Oceanic Engineering* 29(3), 585-594.

Tuncer, I. H. and M. Kaya (2005). Optimization of flapping airfoils for maximum thrust and propulsive efficiency. *AIAA Journal* 43(11), 2329-2336.

Xiao, Q. and W. Liao (2010). Numerical investigation of angle of attack profile on propulsion performance of an oscillating foil. *Computers and Fluids* 39(8), 1366-1380.

Xu, L., F.-B. Tian, J. C. S. Lai and J. Young (2021). Optimal Efficiency and Heaving Velocity in Flapping Foil Propulsion. *AIAA Journal* 59(6), 2143-+.

Young, J. and S. Lai, J. C. (2004). Oscillation frequency and amplitude effects on the wake of a plunging airfoil. *AIAA Journal* 42(10), 2042-2052.

Young, J. and J. C. S. Lai (2007). Mechanisms Influencing the Efficiency of Oscillating Airfoil Propulsion. *AIAA Journal* 45(7), 1695-1702.